Parametric analysis of the area of review (AoR) using CCSNet, a deep-learning-based CO_2 storage modeling tool

Hemanth Hariharan, Sarah Saltzer, Sally M. Benson

Abstract

The Environmental Protection Agency (EPA) developed regulatory requirements and provisions for CO_2 storage in deep geological formations to protect public health and underground sources of drinking water (USDWs) from the unique nature of CO_2 gas such as its buoyancy relative to water, subsurface mobility, corrosivity in the presence of water and large injection volumes. A key element of EPA's regulatory approach, the Area of Review (AoR), is the region surrounding the geological sequestration project where USDWs may be endangered by injection activity. This study uses CCSNet, a deep-learning modeling suite for CO_2 storage, to provide a thorough and comprehensive assessment of the influence of reservoir and operational parameters on the AoR. In addition, we develop a parametric tool and charts for quickly computing the radius of the AoR for idealized homogenous reservoirs, and synthetic heterogeneous reservoirs, and compare our results to AoRs for projects in the permitting pipeline or operational today. The results from this study enable project developers to easily screen sites to identify those with the smallest AoR and develop operational guidelines to limit the AoR, thus expanding the existing framework for site selection and making more informed choices of storage locations by considering the size of the AoR.

Keywords: Area of review, CCSNet, pressure buildup, brine leakage, parametric analysis, nomogram, phase diagram

Introduction

Carbon capture and storage (CCS) is a key technology for reducing carbon dioxide (CO_2) emissions from industrial and energy-producing activities to mitigate climate change (Intergovernmental Panel on Climate Change 2015). One of the major

concerns associated with the injection and storage of CO_2 in deep geologic formations is the potential for leakage and migration of CO_2 or brine into underground sources of drinking water (USDWs) (Tsang et al., 2002; Celia et al. 2011). The potential pathways for such leakages include geologic features such as transmissive faults and fracture systems or manmade pathways such as poorly or improperly plugged wells (Benson et al. 2005; Bielicki et al. 2018).

The EPA defines Class VI wells as those used in long-term storage of underground CO_2 in deep rock formations. The lifecycle of a Class VI project typically involves several stages, from planning and permitting to construction, injection/operation, monitoring, and closure. The area of increased risk to USDWs due to the injection activities is referred to as the Area of Review (AoR). The delineation and evaluation of the AoR is one of the key requirements to fulfill EPA's risk mitigation regulations [Fig 1] and permit class VI projects. Under EPA's regulations, the AoR is defined based on the maximum extent of the separate-phase CO_2 plume and pressure buildup predictions from computational modeling [Fig 2].

The size of the AoR is an important driver of the cost and risk of a storage project and hence is a key determinant of commercial success. The size of the AoR can have a significant impact on project cost, as it will determine the number of legacy wells needing review and possible remediation, the monitoring footprint of the project, and the acreage required. A large AoR requires more resources for site characterization, corrective action, and monitoring and will impact project economics over a long operational period. The evaluation of the AoR could potentially eliminate certain regions from consideration such as those with an unacceptably high density of existing legacy wells. Consequently, the results of this analysis can help direct project developers toward more promising areas that meet the desired criteria. Minimizing the AoR while accounting for and handling the potentially transmissive features within it is crucial to the long-run success of a CCS project (Bump and Hovorka 2023).

The AoR is determined using computational modeling that accounts for the physical and chemical properties of the injected CO_2 stream and displaced fluids and is based on available site characterization, monitoring, and operational data. Owners or operators of injection wells must identify any potential conduits for upward

migration of fluids within the AoR, assess the integrity of these penetrations, and perform corrective action where necessary to prevent fluid leakage into a USDW. Determination of the AoR for proposed Class VI wells consists of data collection and compilation, development of the site computational model, and finally, delineation of the AoR based on the model results. The model parameters for the multiphase fluid modeling of geologic sequestration include hydrogeologic properties (permeability, porosity, temperature, fluid pressure, etc.), fluid properties (viscosity, compressibility, etc.), chemical properties (diffusion coefficient, solubility, etc.), fluid injection and withdrawal rates, system orientation, and simulation controls (number of model layers, layer thickness, grid cell size, model timeframe, time step size, etc.).
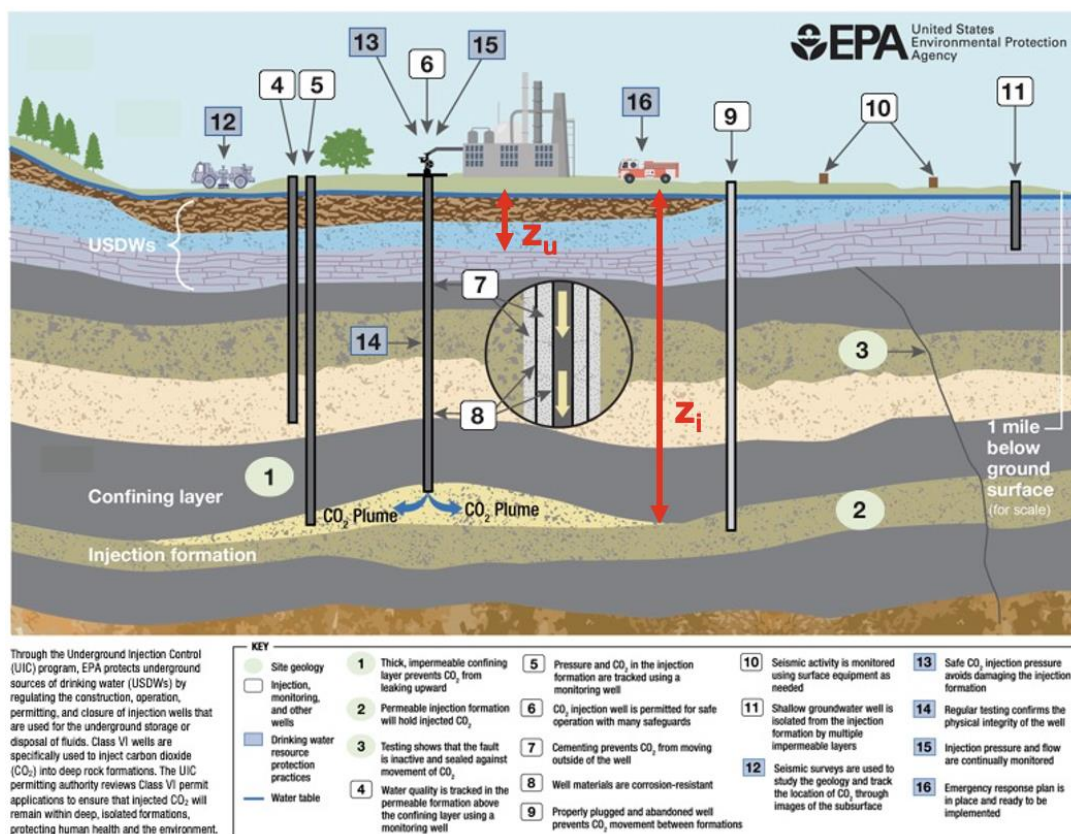

Fig. 1. Graphic showing several aspects of risk mitigation in a Class VI project (from US EPA 2015).

The critical pressure is defined as the minimum pressure within the injection zone necessary to cause fluid flow from the injection zone into the formation matrix of the USDW through a hypothetical open conduit (US EPA 2015). Numerous methods have been proposed for calculating the critical pressure buildup for leakage (Thornhill et al, 1982; Nicot et al. 2009; Birkholzer et al. 2011; Bacon et al, 2020). Here we define the critical pressure radius based on one of two methods accepted by the EPA (US EPA 2013):

$$P_{i,f} = P_u + \rho_i g \cdot (z_u - z_i) \tag{1}$$

where $P_{i,f}$ is the critical pressure in the storage reservoir, P_u is the initial fluid pressure in the USDW, ρ_i is the injection-zone fluid density, g is the acceleration due to gravity, z_u is the representative depth of the USDW, and z_i is the representative depth of the injection zone. Similarly, pressure buildup ($\Delta P_{i,f}$) over the initial reservoir pressure (P_i) that may be sustained in the injection zone is given by:

$$\Delta P_{i,f} = P_u + \rho_i g \cdot (z_u - z_i) - P_i \tag{2}$$

Eq-1 and Eq-2 are subject to the assumptions that the hypothetical open borehole provides a connected pathway for fluid flow between the injection zone and USDW, the fluid in the open borehole has a constant density equal to the density of the fluid in the storage formation (Nicot et al., 2009), and the reservoir is initially not overpressured with respect to the shallow aquifer. A positive value of $\Delta P_{i,f}$ (Eq-2) corresponds to an injection reservoir that is under-pressurized relative to the USDW and can accommodate an increase in pressure equal to $\Delta P_{i,f}$ before potential fluid migration into the drinking water reservoir. Alternatively, when $\Delta P_{i,f}$ is negative, upward flow from the storage reservoir into the USDW would occur. In reality, water density is a function of temperature, pressure, and salinity and typically varies with depth. However, for this study, it was assumed that density decreases caused by the geothermal gradient would be counteracted by the increasing pressure with depth, leading to a constant fluid density with depth as was done in Birkholzer et al. (2011).

To calculate the AoR, it is also necessary to calculate the spatial extent of CO_2 plume (US EPA, 2013). The plume radius is typically calculated using numerical simulation as discussed below. The AoR is then defined as whichever is larger of

the critical pressure radius or the plume radius at that location as is illustrated in Figure 2.
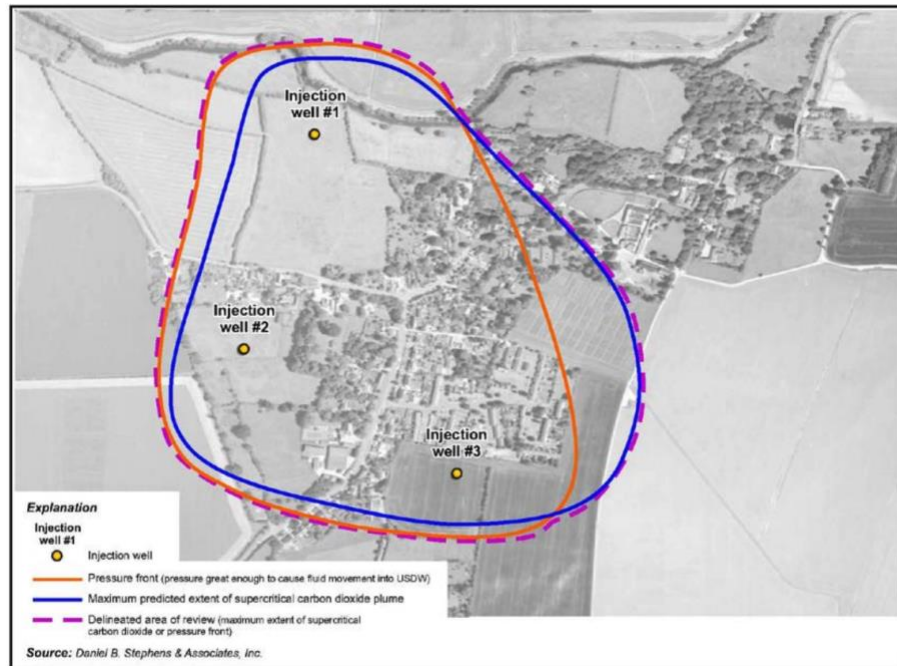

Fig. 2. Hypothetical example of an AoR delineation, using the maximum extent of the CO_2 plume and critical pressure radius (from US EPA 2015)

Numerical simulation based on a detailed geomodel of the storage site is used to calculate the extent of the CO_2 plume and critical pressure radius. Ideally, the model is run using a range of equiprobable realizations of the geomodel to obtain a probabilistic assessment of the AoR as recommended by Pawar et al., (2017). However, numerical simulations for multiphase flow problems are computationally intensive and time-consuming, and may limit the potential for a thorough probabilistic assessment. In addition, during the scoping stage of a project and permit application process for a Class VI well, only limited geological data may be available to characterize the formation, making probabilistic studies even more valuable to the project developer. In the past 5 years, deep learning has shown potential for developing highly computationally efficient methods of solving multiphase flow problems nearly as accurately as traditional methods (Wen et al., 2021; Gupta et al., 2021; Hussin et al., 2023; Lie et al., 2023; Wang et al, 2024).

The goal and novelty of this study is to use CCSNet to provide a thorough and comprehensive assessment of the influence of reservoir and operational parameters on the AoR. In addition, based on results from hundreds of thousands of simulations, we develop a parametric tool and charts for quickly computing the size of the AoR and compare our results to AoRs for projects in the permitting pipeline or operational today. The results from this study enable project developers to easily screen sites to identify those with the smallest AoR and develop operational guidelines to limit the AoR, thus expanding the existing framework for site selection and enabling more informed choices of storage locations by considering the size of the AoR early in screening and scoping studies.

Methods

For this study, we use CCSNet, a deep learning model which was trained using a suite of convolutional neural networks (CNNs) and provides predictions of CO_2 gas saturation distribution, pressure buildups, and other outputs (Wen et al, 2021). CCSNet has been trained and tested over a wide range of reservoir and injection parameters and demonstrated to have a mean pressure error of 2.5% and a mean plume error of 0.9% (Wen et al, 2021). Each pressure buildup and CO_2 plume migration simulation takes 0.04 and 0.05 s, respectively, thus enabling a large number of scenarios to be evaluated (Wen et al., 2021). To carry out the simulations, we use CCSNet's backend application programming interface (API) for a 2D-radial isotropic model to run hundreds of thousands of trials in both homogeneous and synthetic heterogeneous reservoirs.

The radius of the AoR was computed over a wide range of possible storage reservoir properties and initial conditions as summarized in Table 1. Note that we assume a constant geothermal gradient, water table depth, and surface temperature for calculating the initial reservoir temperature and pressure. For the first set of calculations, we assume the storage reservoir is homogeneous and isotropic. The AoR for a total of 766,020 scenarios is evaluated for the first set of calculations. In a second series of scenarios, we simulate 1000 heterogeneous reservoirs with a broad range of properties to determine how reservoir heterogeneity impacts the conclusions determined from the first phase of the study (see Table 5).

Parameter/Output	Unit	Symbol	Minimum	Maximum	Step Size	# of values
Brine density	kg/m^3	ρ_{brine}	1020	1100	20	10
Injection Rate	MT/year	Q	0.25	2	0.25	8
Depth to bottom of USDW	m		100	350	50	6
Depth to the top of the reservoir	m		800	1800	100	12
Reservoir thickness	m	h	50	200	25	7
Reservoir permeability	mD	k	50	1000	50	19
Water Table Depth	m		10		Constant	
Geothermal Gradient	ºC/km		25		Constant	
Surface Temperature	ºC		15		Constant	
Radius of AoR	m	r_a				
Radius of CO$_2$ plume	m	r_{plume}				
Radius of critical pressure region	m	$r_{pressure}$				
Depth from the bottom of the USDW to the top of the reservoir	m	z				
Difference in brine and water densities	kg/m^3	$\rho_{brine} - \rho_{water} = \Delta\rho$				

Table. 1. Range and step sizes of variables and outputs for the parametric analysis of the AoR.

To calculate the AoR for each simulation, we first calculate the critical pressure using Eqs. 1 and 2. The critical pressure is calculated for a range of brine densities, from 1020 to 1100 kg/m³, corresponding to a range of salinities from about 25,000 to 150,000 ppm. After running CCSNet to simulate 20 years of injection, the CO_2 maximum plume radius and the critical pressure radius are extracted from the simulations. Specifically, the plume radius at the end of 20 years is determined from the maximum distance that the supercritical CO_2 plume has migrated away from the injection well. The critical pressure radius is the maximum distance from the injection well, where the pressure buildup at the top of the reservoir was greater than or equal to the critical pressure buildup (Eq. 2). The AoR radius is then computed as the maximum of the plume and critical pressure radius.
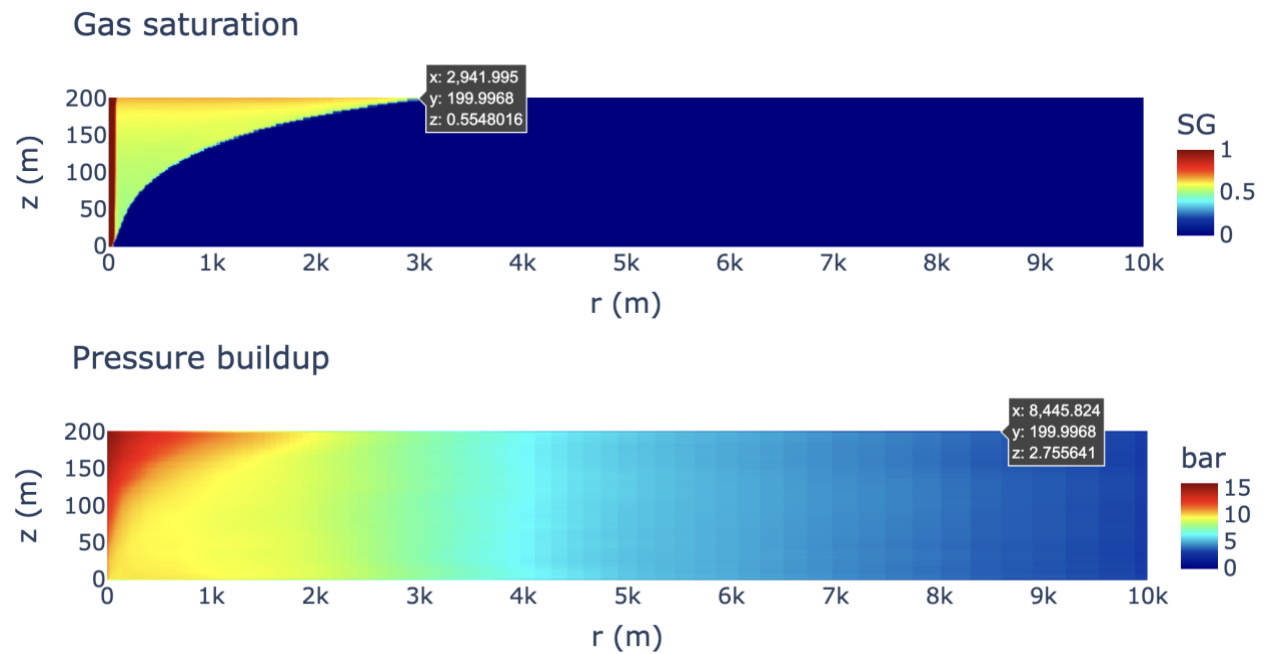

Fig. 3. Example output from CCSNet from which the plume radius and critical pressure radius are extracted. The cursor in the gas saturation diagram is positioned near the plume radius (~ 3000 m), representing the maximum extent of supercritical CO_2. The cursor in the pressure buildup diagram is placed near the critical pressure radius (~ 8,500 m), where pressure buildup at the top of the reservoir (~ 2.75 bar) exceeds the critical pressure build as calculated from Eq. 2.

Results

Key features of these simulations are illustrated in Figure 4 using an interactive parametric tool (link provided in 'Code and Data Availability' section) to visualize

the CO_2 plume radius, critical pressure radius, and resulting AoR radius as a function of 4 parameters: permeability, injection rate, brine density, and reservoir thickness. The values of the parameters kept constant are detailed in Table 2. For example, in Fig 4A, we see that all else being equal, in thin reservoirs the critical pressure radius is much larger than the plume radius – henceforth referred to as a pressure-dominated AoR. However, as the reservoir thickens and therefore has a larger volume to accommodate the injected CO_2, the critical pressure decreases. Eventually, for a thick enough reservoir, the radius of the plume exceeds the critical pressure radius and the AoR becomes plume-dominated.

The influence of brine density on the AoR is shown in Fig 4B. For low brine densities, the AoR is pressure-dominated and large. As the brine density increases, the critical pressure increases, thus decreasing the AoR. Eventually, as the density increases, the AoR becomes plume-dominated.
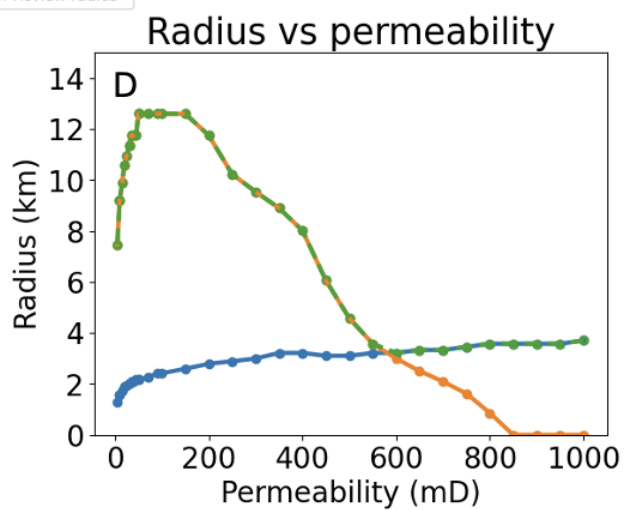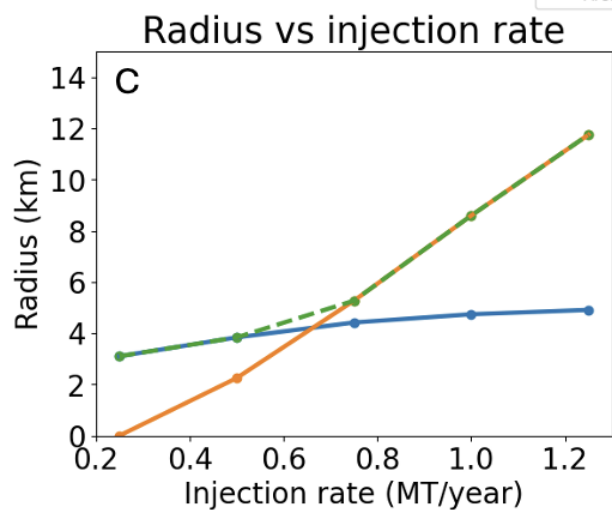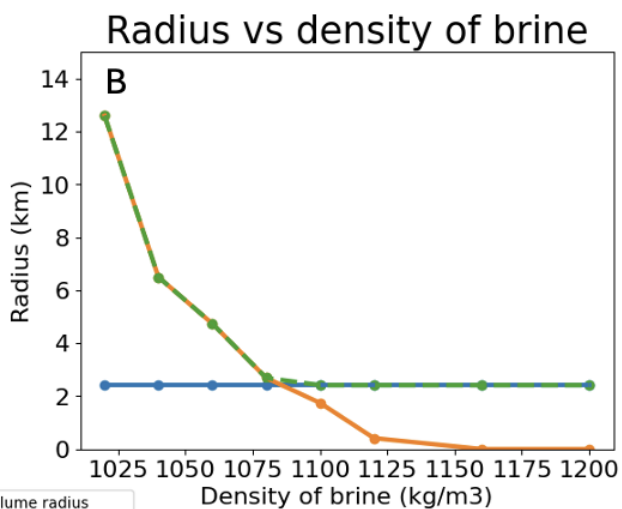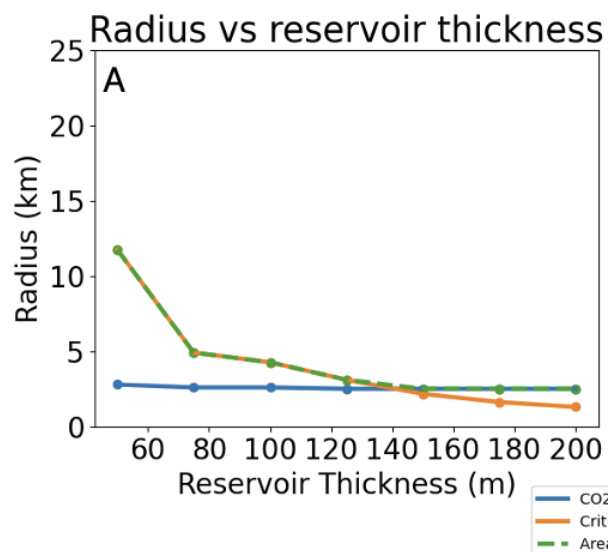
Increasing the injection rate can cause a plume-dominated AoR to become a pressure-dominated AoR as shown in Figure 4C. For low injection rates, the pressure buildups may not exceed the critical pressure buildup and thus the AoR is by definition plume-dominated. However, with increasing injection rates, the critical pressure may be exceeded.

Permeability has a large impact on both plume migration and pressure buildup as shown in Figure 4D. For permeabilities in the range of 150 mD, plume migration is dominated by viscous forces and is fairly compact, with a size of around 2500 m (see insert in 4D). At high permeabilities, plume migration is strongly influenced by buoyancy, driving CO_2 to the top of the reservoir and spreading under the seal. This leads to larger plumes, with a size of around 3500 m as shown in Fig. 4D. For low permeabilities, the AoR is pressure-dominated and much larger than the plume. As shown, interestingly, the size of the AoR is not monotonic as might be expected. The non-monotonic behavior results from a combination of processes, including the influence of pressure buildup on the density of CO_2 and the lower pressure diffusivity ($k/\phi\mu c_t$) for low permeability formations, which confines the pressure buildup nearer to the injection well, and viscous forces (μ/k). Eventually, as the permeability increases, the AoR becomes plume-dominated.

Based on these results, it is clear that depending on the specific reservoir parameter, the project will fall into one of three regimes: pressure-dominated, transitional, or plume-dominated. In general, pressure-dominated AoRs will be the largest and plume-dominated AoRs the smallest.

Scenario		A	B	C	D
Parameter	Unit	Value			
Brine density	kg/m^3	1020	Variable	1020	1020
Injection Rate	MT/year	0.25	0.25	Variable	0.25
Depth to bottom of USDW	m	100	100	100	100
Depth to the top of the reservoir	m	800	800	800	800
Reservoir thickness	m	Variable	50	125	50
Reservoir permeability	mD	200	100	500	Variable

Table. 2. Values of parameters kept constant while varying one of the independent variables in each of the scenarios shown in Figure 4.

Radius vs reservoir thickness

A

Radius vs density of brine

B

Radius vs injection rate

C

Radius vs permeability

D

Legend:
— CO2 plume radius
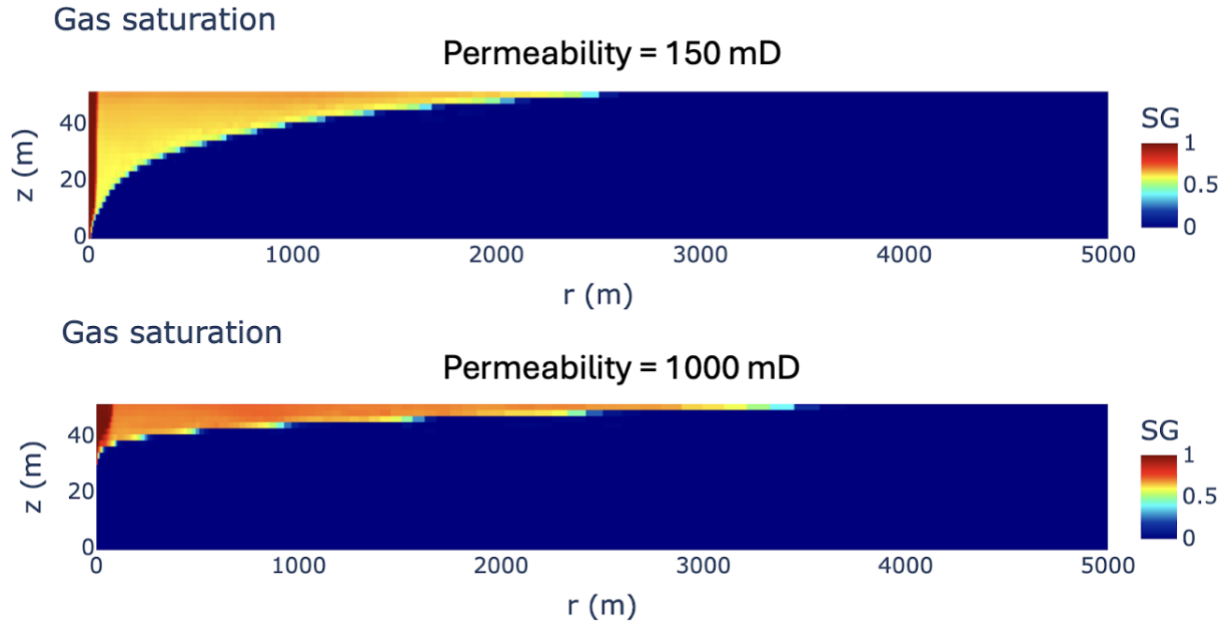— Critical pressure radius
-- Area of Review radius

Fig. 4. Output of the parametric tool to observe the size of the CO_2 plume, critical pressure, and AoR as a function of (A) reservoir thickness, (B) brine density, (C) injection rate, and (D) reservoir permeability. All of these calculations are for the end of the 30-year injection period. In addition, for 4(D), the gas saturation diagrams have also been included to highlight the difference in plume sizes for two extreme permeability cases. A permeability of 150 mD leads to a plume radius of around 2500 m while a permeability of 1000 mD leads to a plume radius of around 3500 m, which aligns with the results observed in 4(D). See Table 2 for the parameters used in the scenarios A-D.
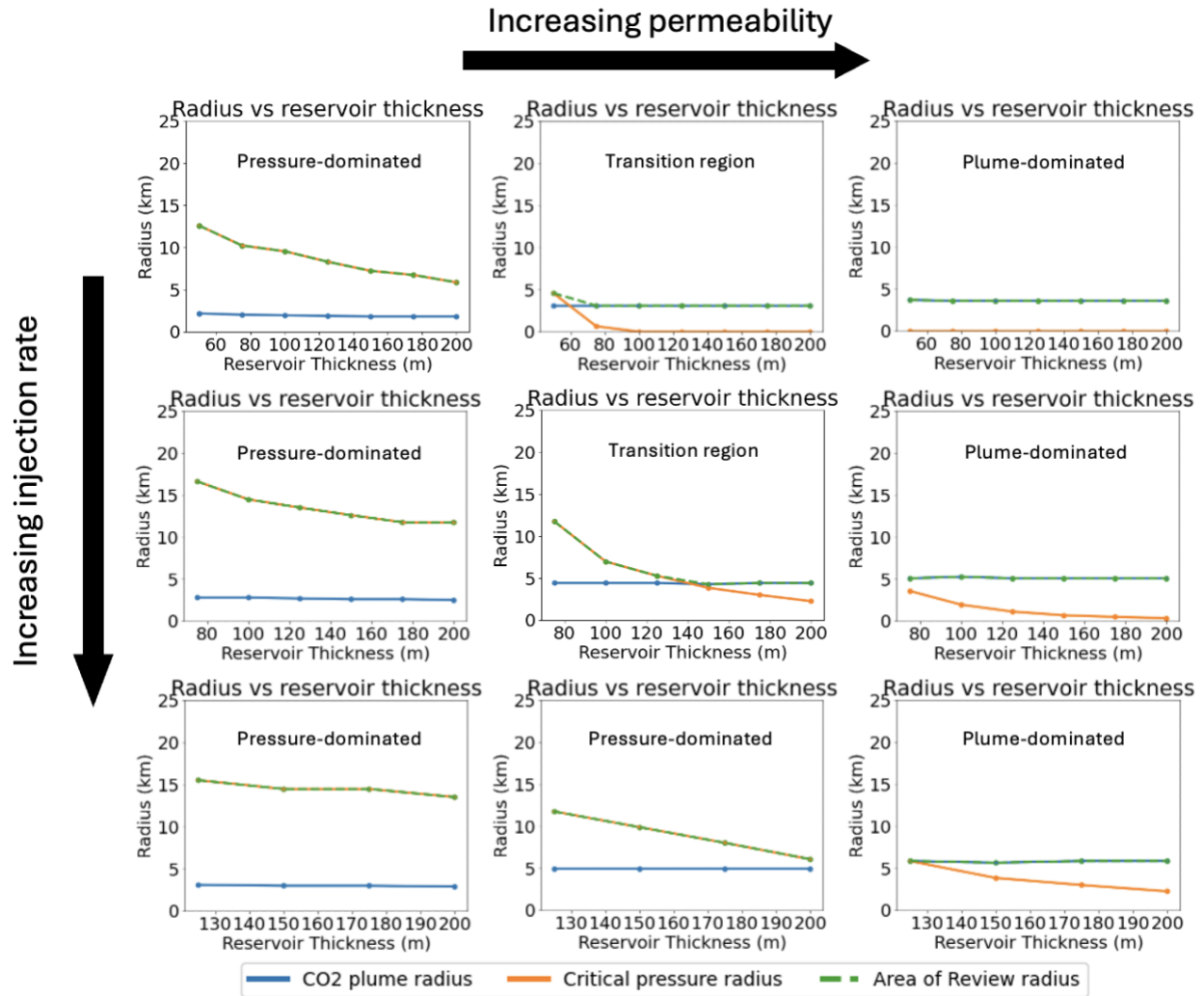
Fig. 5. Sensitivity plots of CO_2 plume radius, critical pressure radius, and the AoR radius as a function of reservoir thickness (Fig. 4A) for varying permeabilities and injection rates. These are for permeabilities of 50 mD, 500 mD, 1000 mD, and injection rates of 0.25 MT/year, 0.75 MT/year and 1.25 MT/year. The brine density, depth to the bottom of the USDW, and depth to the top of the reservoir are kept constant at 1020 kg/m³, 100 m, and 800 m respectively.

Fig. 6. Sensitivity plots of CO_2 plume radius, critical pressure radius, and the AoR radius as a function of injection rate (Fig. 4C) for varying permeabilities and thicknesses. These are for permeabilities of 50 mD, 500 mD, 1000 mD and thicknesses of 75 m, 125 m and 175 m. The brine density, depth to the bottom of the USDW and depth to the top of the reservoir are kept constant at 1020 kg/m^3, 100 m and 800 m respectively.
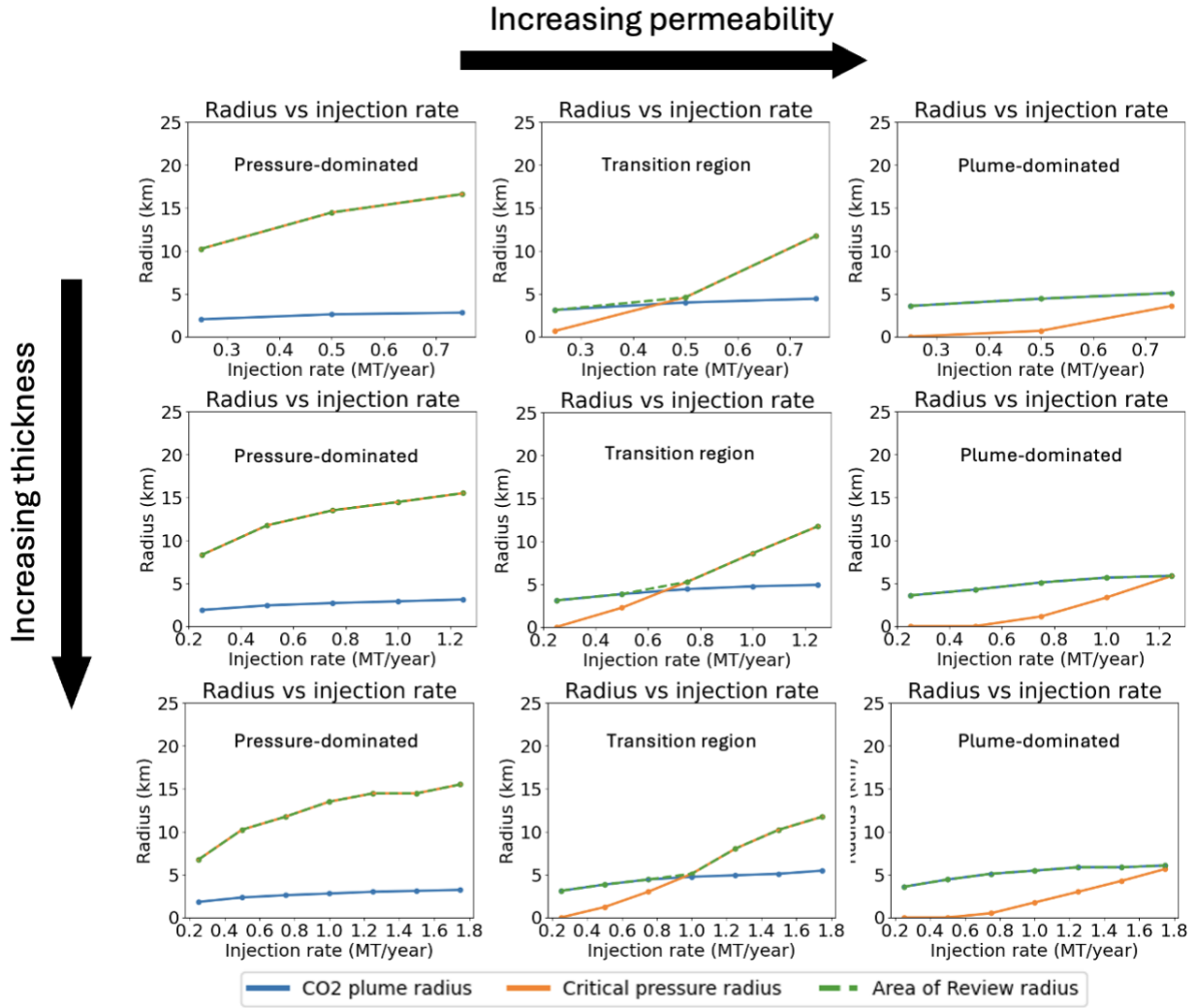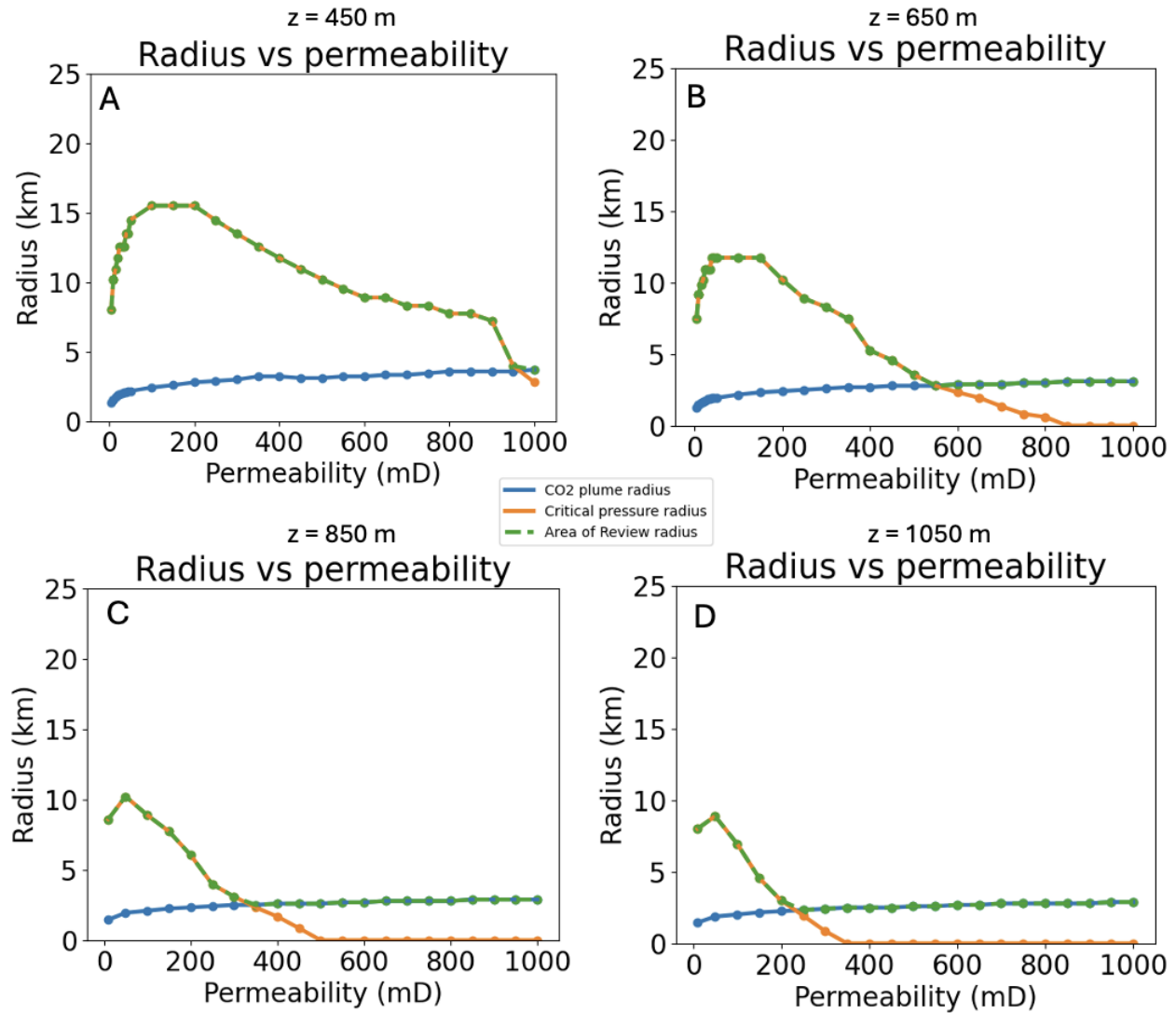
Fig. 7. Sensitivity plots of CO_2 plume radius, critical pressure radius, and the AoR radius as a function of permeability for varying separations between the bottom of the USDW and the top of the reservoir. These are for depths to the top of the reservoir of 800 m, 1000 m, 1200 m, and 1400 m. The brine density, injection rate, reservoir thickness, and depth to the bottom of the USDW are kept constant at 1020 kg/m^3, 0.25 MT/year, 50 m, and 350 m respectively.

The essential features of the relationship between the reservoir parameters, operational parameters, and ratio between the r_{plume} and $r_{pressure}$ can be captured in a 2-dimensional plot (Figure 8).

The gradual progression of the ==nomogram== from low values of $k_{av}h/Q$ to higher values of $k_{av}h/Q$ is observed in Figure 8. A low $k_{av}h/Q$ is generally indicative of a combination of a thin reservoir, with low permeabilities and/or high injection rates. These conditions typically lead to large pressure buildups, which are characterized by high critical pressure radii. ==As shown, for low values of $z\Delta\rho g$ (<2 bar), the ratio of $r_{pressure}/r_{plume}$ is greater than one for all values of kh/Q greater than 9 x 10^{-11} m^3/MT/year, indicating the AoR is pressure dominated.== On the contrary, a high $k_{av}h/Q$ is generally indicative of a combination of a thick reservoir, with high permeabilities and/or low injection rates. In the above conditions, the pressure buildup is low and the critical pressure buildup required for leakage is observed to occur close to the injection well. In such scenarios, the plume governs the AoR, leading to a $r_{pressure}/r_{plume}$ that is less than unity.

The nomogram enables project developers to perform early-stage estimates of the size of the AoR to evaluate the economic viability of potential CCS projects. A hypothetical project (see Table 3) is considered to illustrate the use of the nomogram in practice. The assumed set of parameters leads to an estimated range of $k_{av}h/Q$ between 2e-11 and 3e-11 m^3/MT/year. $z\Delta\rho g$ is computed to be 3.43 bars. This corresponds to a range of $r_{pressure}/r_{plume}$ between 3 and 5.5. A project developer looking to minimize the size of the AoR can thus choose an injection rate of 0.5 MT/year which would reduce the radius of the critical pressure region by 45% (from around 5.5 times the plume radius to around 3 times the plume radius), thus moving the project from point A to point B on the nomogram along the solid black arrow. The nomogram hence provides a tool to select an optimal injection rate subject to other practical constraints, to minimize the size of the AoR.

Parameter	Symbol	Value	Unit
Mean reservoir permeability	k_{av}	1.5×10^{-13}	m^2
Depth from the bottom of USDW to the top of the reservoir	z	500	m
Reservoir thickness	h	100	m
Difference in brine and water densities	$\rho_{brine} - \rho_{water} = \Delta\rho$	70	kg/m^3

Injection rate	Q	0.5 - 0.67	MT/year

Table. 3. Symbols, units, and values of parameters used to triangulate the hypothetical project on the nomogram
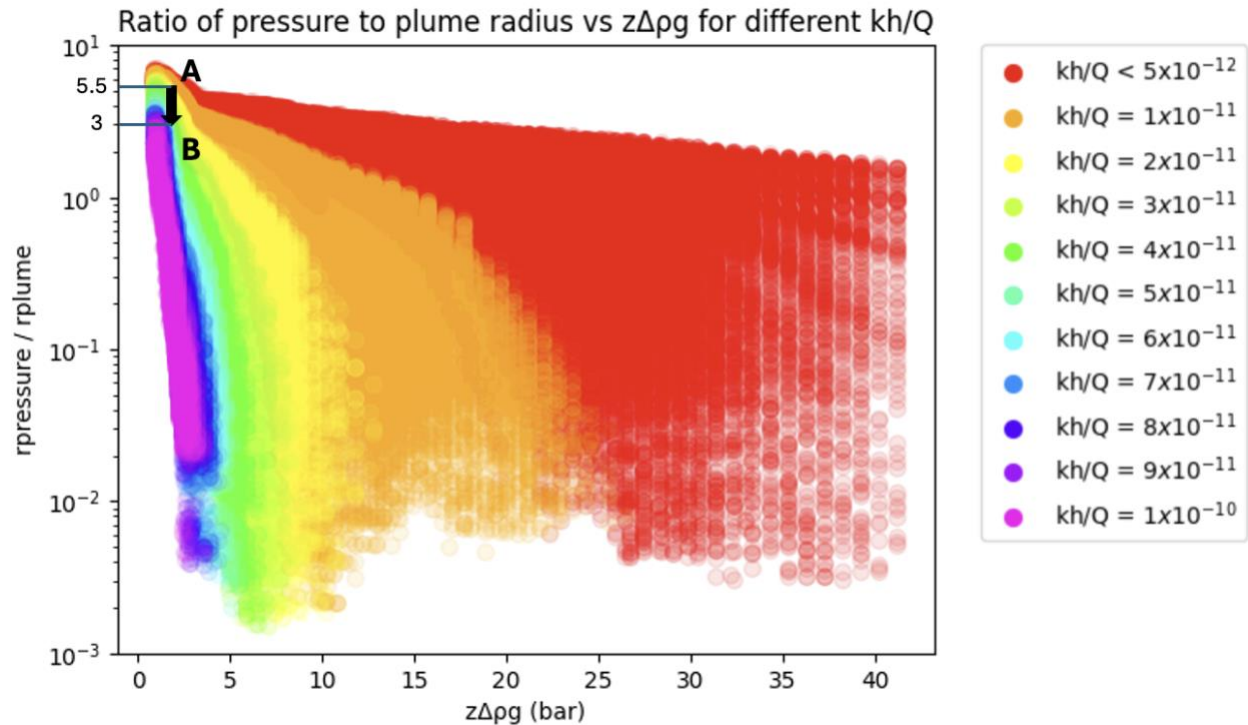

Fig. 8. Ratio of the critical pressure radius to that of CO_2 plume vs $z\Delta\rho g$ for different values of $k_{av}h/Q$.

A histogram was plotted (see Figure 9) for CO_2 plume and pressure-dominated scenarios to understand the distribution of the AoR radii. The plot confirms the well-known observation that the critical pressure region generally extends well beyond the CO_2 plume. Pressure changes in the subsurface tend to propagate much farther than the actual migration of injected CO_2 because pressure transmission through the pore network occurs quicker compared to fluid movement, which is constrained by factors like capillary forces and permeability. Consequently, larger land areas will be affected in projects whose AoR are pressure-defined.
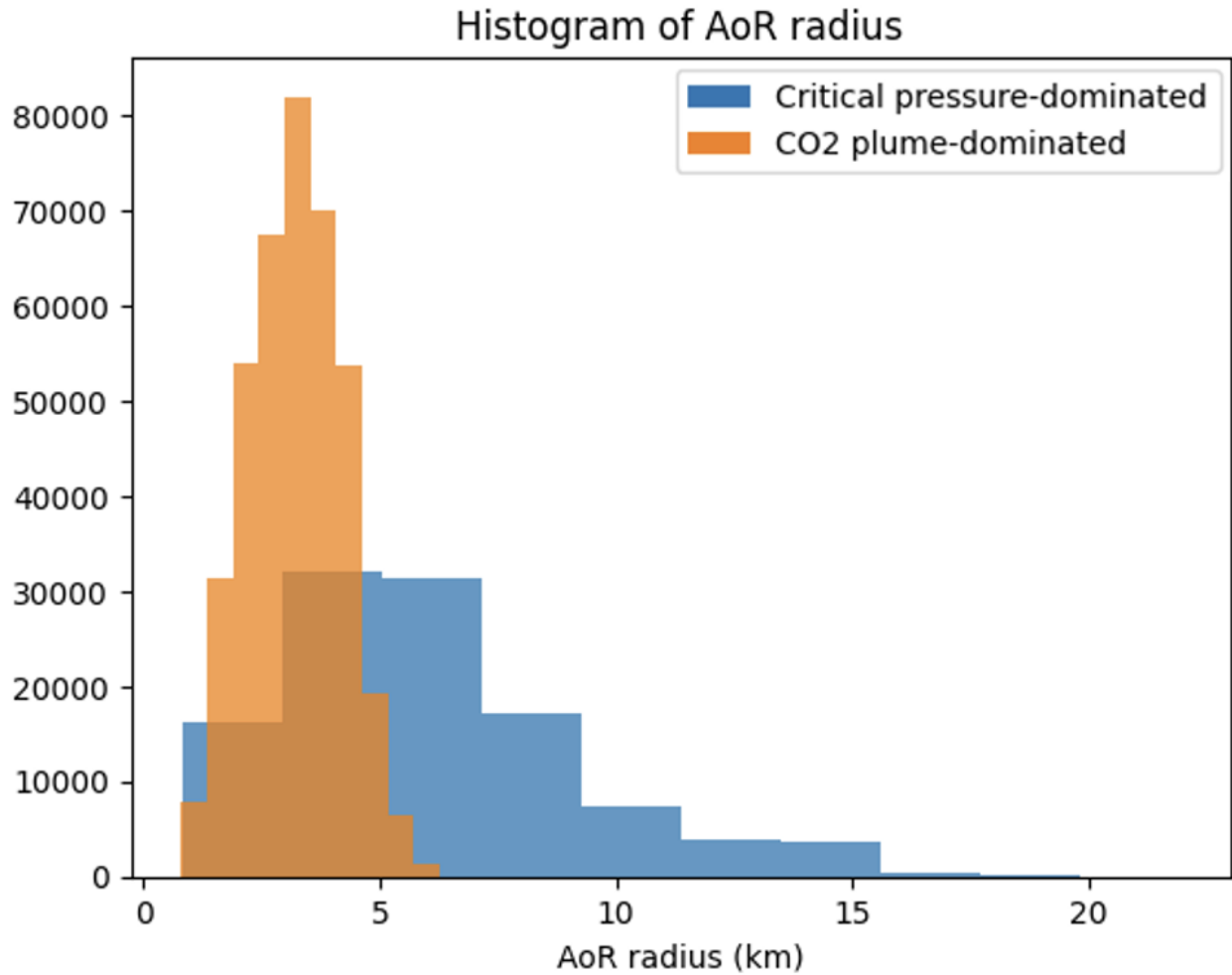
Fig. 9. Histogram of AoR radius region (in blue) where the critical pressure governs the AoR and the region (in orange) where the CO_2 plume governs the AoR.

A graphical representation of the governance of the AoR under different combinations of $k_{av}h/Q$ and $z\Delta\rho g$ is represented by a "phase diagram" in Figure 10. Similar to the interpretation of small and large values of $k_{av}h/Q$ as mentioned earlier, a small value of $z\Delta\rho g$ represents a combination of a small difference in depth between the bottom of the USDW and the top of the reservoir and a small difference in brine and water densities. Likewise, a large value of $z\Delta\rho g$ can be interpreted as a combination of large depth and density differences.

The phase diagram indicates governance of the AoR by the critical pressure radius for small values of $k_{av}h/Q$ and $z\Delta\rho g$. This is consistent with the large pressure buildups associated with a small $k_{av}h/Q$, which when coupled with a small $z\Delta\rho g$, would lead to a critical pressure buildup for leakage only to occur at a significant

distance from the injection well. On the other hand, the AoR is governed by the CO_2 plume for large values of $k_{av}h/Q$ and $z\Delta\rho g$. A large $k_{av}h/Q$ leads to a small pressure buildup, which in the scenario of a large $z\Delta\rho g$, leads to a critical pressure buildup that occurs very close to the well.

Class VI Project	Wells	k_{av} (mD)	h (m)	Q (MT/y)	z (m)	$\Delta\rho$ (kg/m³)	Critical pressure (bar)	AoR (permit)	AoR (phase diagram)
HGCS LLC, Vervain	2[1]	107[1]	69[1]	2.50[1]	1005.31[1]	58.63[1]	9.45[2]	Pressure[1,2]	Pressure
ADM - Decatur Campus	4[3]	185[3]	22.5[3]	1.1[3]	953[4]	124[4]	4.29[3]	Pressure[4]	Pressure
Lorain Carbon Zero Solutions, LLC	1[5]	9.4[5]	27[5]	0.12[5]	1426[5]	25[5]	3.50[5]	Pressure[5]	Pressure
Wabash Carbon Services	2[6]	2400[6]	235.2[6]	0.83[6]	119[6]	29.99[6]	0.35[6]	Plume[6]	Plume
HGCS LLC, Christian County	6[7]	9.19e-4 to 1.82[7]	283.5[7]	6[7]	-	-	9.31[8]	Pressure[8]	Pressure
Oxy Low Carbon Ventures, LLC Brown Pelican	3[9]	12.4[9]	210[10]	0.73[10]	1056[10]	105.76[10]	10.96[10]	Combination[10]	Pressure (close to transition)
CTV Elk Hills A1-A2	2[11]	108[11]	61.2[11]	0.25 to 0.75[11]	2328[11]	11[11]	2.51[11]	Plume[11]	Transition
CTV Elk Hills 26R	4[12]	64.05[12]	947.71[12]	1.45[12]	-	-	0.69[12]	Plume[12]	Pressure (close to transition)
CTV Holdings: CTV III	6[13]	71.7[13]	307.21[13]	2.5[13]	1050[13]	5.72[13]	0.59[13]	Pressure[13]	Pressure

[1] Heartland Greenway Carbon Storage - Class VI permit Application Narrative (pages 11, 54, 74, 98 of 104)

[2] Heartland Greenway Carbon Storage Class VI permit - Area of Review and Corrective Action Plan (pages 38, 48 of 60)

[3] Archer Daniels Midland - UIC Program Class VI Well for Geological Sequestration of Carbon Dioxide (pages 8, 64, 103 of 328)

[4] Archer Daniels Midland - Attachment B: Area of Review and Corrective Action Plan (pages 10, 11, 14 of 20)

[5] Lorain Carbon Zero Solutions LLC - Class VI Permit Application Narrative (pages 27, 118, 122, 136 of 165)

[6] Wabash Carbon Services - Underground Injection Control Permit Class VI (pages 34, 37, 40, 41 of 109)

[7] Heartland Greenway Carbon Storage - Class VI Permit Application Narrative (pages 6, 22, 29 of 55)

[8] Heartland Greenway Carbon Storage - Area of Review and Corrective Action Plan (pages 32, 37 of 46)

[9] Brown Pelican CO2 Sequestration Project - Class VI Permit Application Narrative (page 5 of 751)

[10] Oxy Low Carbon Ventures LLC - Class VI permit (pages 78, 80, 81, 83, 87, 91, 109 of 242)

[11] Carbon TerraVault 1 LLC Elk Hills A1-A2 Storage Project - Class VI Permit Application Narrative (pages 1, 17, 21 of 45) and Class VI critical pressure calculation (pages 3, 4 of 4)

[12] Carbon TerraVault Elk Hills 26R - Class VI draft permit (pages 44, 46, 53, 57, 65 of 177)

[13] Carbon TerraVault III Class VI permit application Narrative Report (pages 4, 28, 30, 125 of 133) and Area of Review and Corrective Action Plan (pages 5, 24, 32 of 58)

Aera Energy LLC: CarbonFrontier	9[14]	47.19[14]	180[14]	3.285[14]	2175[14]	16[14]	3.41[14]	Pressure[14]	Pressure
Pelican Renewables, LLC	2[15]	250[15]	60 to 690[15]	2.02[15]	575[15]	9.17[15]	10[15]	Combination[15]	Plume (partly in transition)
Montezuma NorCal CarbonSequestration Hub	1[16]	20 to 200[16]	396.3[16]	1[16]	2867[16]	7[16]	1.97[16]	Pressure[16]	Pressure
Chevron USA Inc, Kern River Eastridge CCS	4[17]	2000[17]	315[17]	0.27 to 0.46[17]	1396.2[17]	3.56[17]	0.49[17]	Plume[17]	Plume
Tallgrass: Eastern Wyoming Sequestration Hub	1[18]	337[18]	16.29[18]	1.5[18]	2517.3[18]	224.26[18]	55.38[18]	Plume[18]	Plume
Frontier Carbon Solutions LLC	3[19]	2.5[19]	255[19]	1.26[19]	2196.9[19]	17.5[19]	3.77[19]	Pressure[19]	Pressure
Casper Carbon Storage	1[20]	140[20]	67.8[20]	0.4[20]	1461.3[20]	7.21[20]	1.03[20]	Pressure[20]	Pressure
Red Trail Energy, LLC	1[21]	471[21]	93.9[21]	0.18[21]	1192.2[21]	5[21]	0.58[21]	Plume[21]	Plume (partly in transition)

Table. 4. List of projects plotted on the phase diagram in Figure 10 to test practical applicability

[14] Carbon Frontier/Aera Energy LLC Class VI permit application Application Narrative (pages 38, 70, 135, 140 of 2087) and Area of Review and Corrective Action Plan (pages 10, 18, 54 of 286)

[15] Pelican Renewables LLC Class VI permit Application Narrative (pages 3 of 204) and Area of Review and Corrective Action Plan (pages 5, 14, 19, 44, 46, 49, 52, 54 of 74)

[16] Montezuma NorCal Carbon LLC Class VI permit Area of Review and Corrective Action Plan (pages 7, 9, 10, 22, 24, 25 of 44)

[17] Chevron Kern River Eastridge CCS Project Class VI permit Application Narrative (pages 1, 90, 92, 155 of 242) and Area of Review and Corrective Action Plan (pages 32, 43-47 of 332)

[18] Tallgrass Eastern Wyoming Sequestration Hub Class VI permit (pages 33, 100, 166, 306, 307 of 548)

[19] Frontier Carbon Solutions, LLC Sweetwater Carbon Storage Hub Class VI permit (pages 102, 126, 128-130, 949 of 1060)

[20] Casper Carbon Capture, LLC Class VI permit (pages 8, 32, 128, 370, 371 of 374)

[21] Red Trail Energy, LLC Class VI permit (pages 562, 578, 579, 580, 595, 1056, of 1076)

To test the predictive ability of this plot, average values of permeability, reservoir depth, injection rates, depth to USDW, and brine densities were obtained at a number of CCS project sites in the US to understand the governance of the AoR in practice (see Figure 10 and Table 4). For projects where the average permeability, injection rate, or thickness was unavailable, ranges (represented by vertical lines in the phase diagram) were used. Projects that lay outside the domain of the phase diagram are represented using arrows. In some projects, the critical pressure ($z\Delta\rho g$) was explicitly mentioned in the permit, while in other projects, it was computed from z and $\Delta\rho$. For projects where brine and USDW fluid densities were not explicit, salinities were converted to densities using an equation of state (Millero et al. 1980). For projects having multiple injection wells with a unified AoR (Eg. Project 1 - Heartland Greenway Carbon Storage LLC, Vervain, and Project 15 - Frontier Carbon Solutions), individual injection rates were summed up to obtain the total injection rate. For projects with separate AoRs for each well (Eg. Project 4 - Wabash Carbon Services), individual wells were treated separately with their injection rates.

Of the 89 project Class VI permit applications tracked by the EPA or a state with primacy, 16 projects had sufficient publicly available data for assessment, while the other projects were either very early-stage, had withdrawn, used a risk-based approach to determine the AoR, or did not have publicly accessible permit documents. An additional project formerly tracked by the EPA also had adequate data for the analysis, leading to a total of 17 projects that could be plotted on the phase diagram.

The phase diagram enables project developers to predict whether the AoR is CO_2 plume-governed or pressure-governed for an early-stage project purely based on the average permeability, the thickness of the reservoir, injection rate, depth to USDW, and brine density. This information can potentially be used to filter out projects whose economics are very sensitive to the size of the AoR, in which case, a smaller AoR governed by the CO_2 plume would be preferred. It can also be used to estimate the minimum change in $k_{av}h/Q$ required to move a project from the pressure-dominated region to the plume-dominated region. Considering the ADM Decatur project (project 2 boxed in red, in Figure 10) that lies in the pressure-dominated region of the phase diagram, the solid black arrow (that corresponds to an increase of about half an order of magnitude) indicates the minimum change in kh/Q required

to shift it to the plume-governed region of the phase diagram. In practice, this is achieved by selecting sites with thicker, more permeable reservoirs, or by decreasing injection rates.
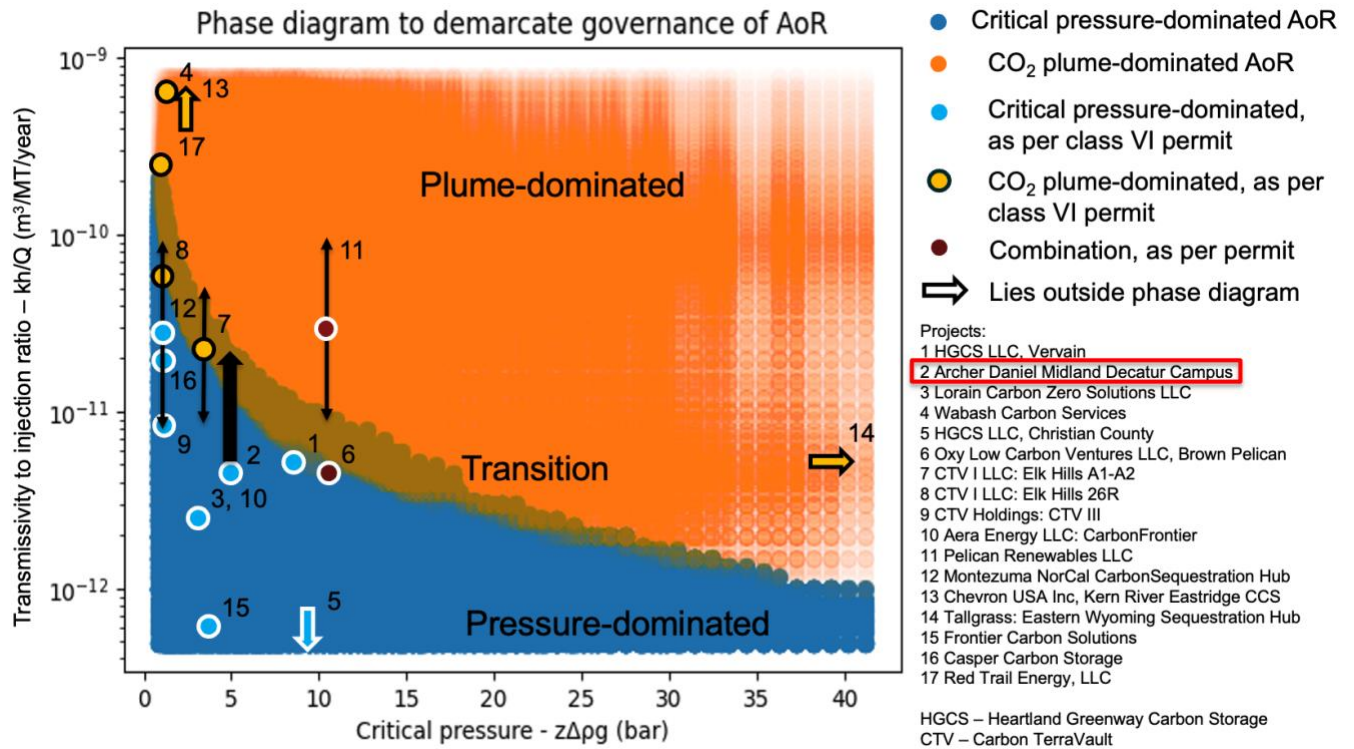

Fig. 10. "Phase-diagram" of $k_{av}h/Q$ vs $z\Delta\rho g$ showing the region (in blue) where the critical pressure governs the AoR and the region (in orange) where the CO_2 plume governs the AoR. 17 CCS project locations are also marked to provide real-world context.

Influence of Heterogeneity on the AoR

Pawar et al., 2016 showed by using 29 equiprobable realizations of a statistically identical reservoir that the AoR is highly sensitive to the degree of geological heterogeneity in the storage reservoir. To further explore this issue over a broader range of scenarios, 1000 cases were run on CCSNet's 2D isotropic model with a synthetic heterogeneous permeability field map for two different mean permeabilities, 100 and 500 md. The permeability fields were generated using SGEMS with a Gaussian permeability field (Remy et al., 2009). The injection rate, depth from the bottom of the USDW to the top of the reservoir, and reservoir thickness are chosen fixed at 1 MT/year, 1400 m, and 100 m respectively while the

other parameters were randomly sampled as shown in Table 5. It is to be noted that in addition to the parameters that were fixed as per Table 2, a constant brine density of 1020 kg/m^3 was assumed for this analysis.

Parameter	Type of distribution	Range of distribution	Unit
The ratio of standard deviation to mean permeability	Uniform continuous	(0, 0.5)	-
Vertical correlation length (λ_v)	Uniform continuous	(2, 10)	m
The ratio of lateral to vertical correlation length	Uniform continuous	(5, 50)	-
Random seed for synthetic field	Uniform discrete (integers only)	(1, 12345)	-

Table. 5. Random sampling of parameters to study the impact of heterogeneity on CO_2 plume and critical pressure radius

Two separate sets of cases were run with mean permeabilities of 100 mD and 500 mD to account for critical pressure-dominated and CO_2 plume-dominated scenarios respectively.
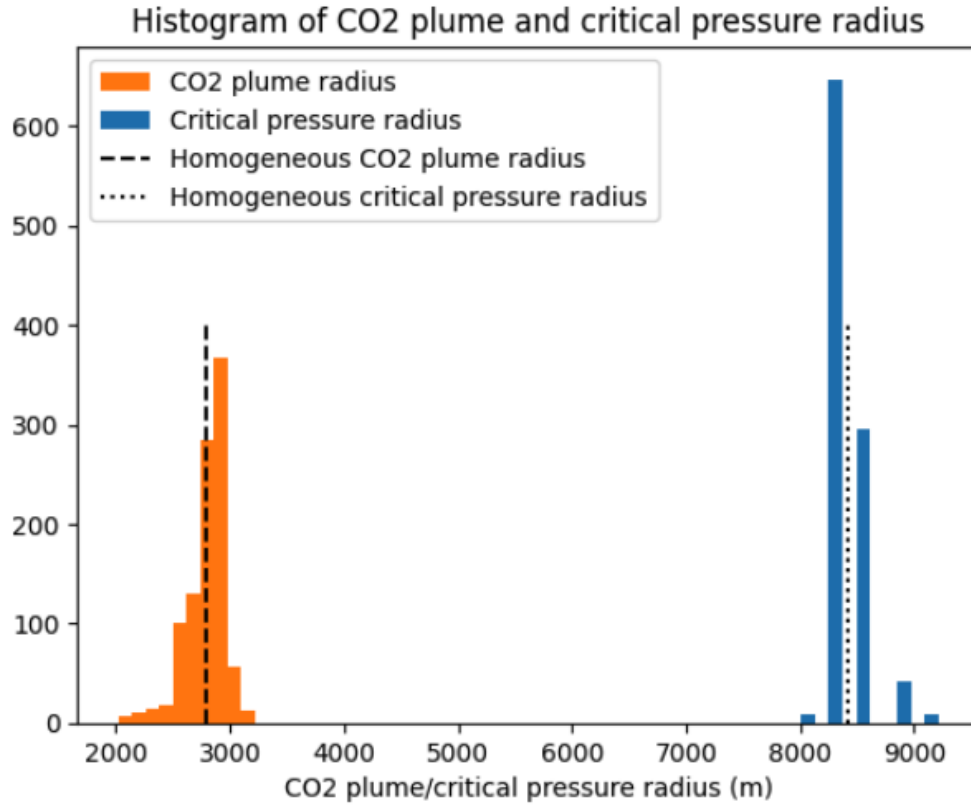
Fig. 11. Histograms of the CO_2 plume and critical pressure radius for 1000 random samples of heterogeneous permeability field maps with a fixed mean permeability of 100 mD

As seen in Figure 11, a mean plume radius of ~2782 m with a standard deviation of ~162 m was observed, while a mean critical pressure radius of ~8415 m with a standard deviation of ~185 m was observed. The ratio of the standard deviation to the mean of the plume radius was 5.84%, while that of the critical pressure radius was 2.2%.

Fig. 12. Histograms of the CO_2 plume and critical pressure radius for 1000 random samples of heterogeneous permeability field maps with a fixed mean permeability of 500 mD

Figure 12 shows the opposite trend, where a mean plume radius of ~3674 m with a standard deviation of ~217 m was observed, while a mean critical pressure radius of ~786 m with a standard deviation of ~224 m was observed. The ratio of the standard deviation to the mean of the plume radius was 5.9%, while that of the critical pressure radius was 28.6%.
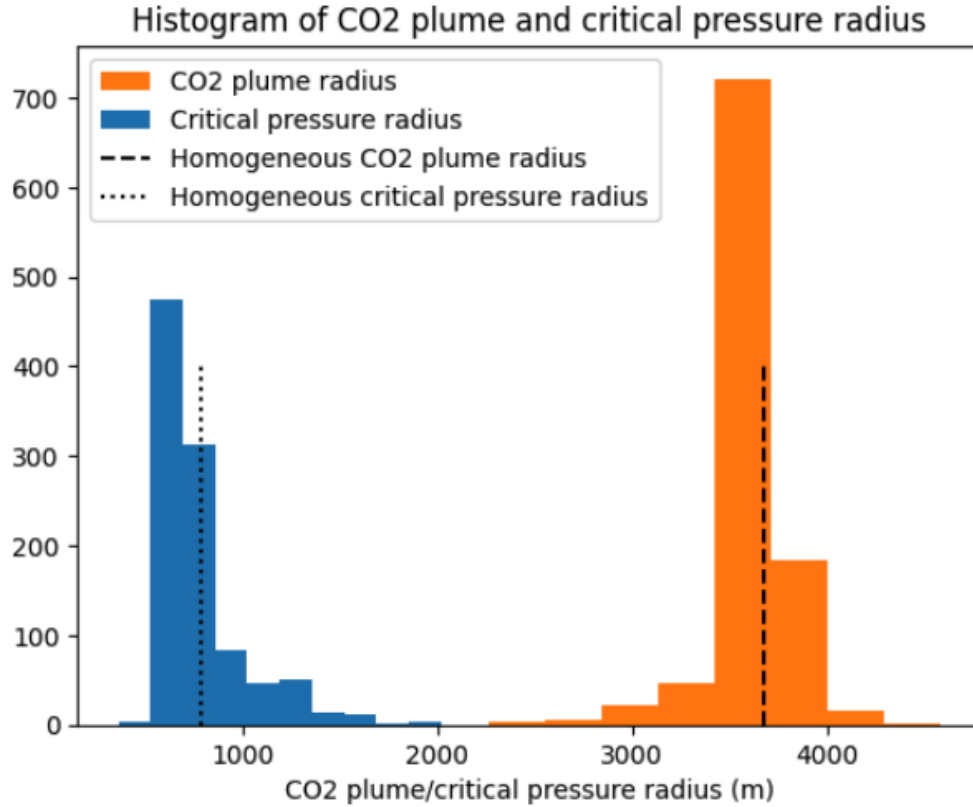
Discussion

There are a number of key insights that can be drawn from the above exercise using the parametric tool developed in this study, and the nomogram and phase diagram plots.

For low injection rates and reservoirs with high permeabilities and high thicknesses, pressure buildup tends to occur only near the injection well, leading to a plume-dominated AoR (see upper right-hand corner of Figure 6). With an increasing

permeability, a transition from a critical pressure-defined AoR to a CO_2-plume-defined AoR is observed, especially at larger reservoir thicknesses. With an increasing injection rate, a critical pressure-defined AoR dominates, except at high permeabilities and large reservoir thickness (see Figure 6). Hence low injection rates and thicker, highly permeable reservoirs are preferred to keep the pressure buildup low and minimize the radius of the AoR. Lower injection rates lead to a more localized pressure perturbation, confining the AoR to a smaller region around the injection well. Thicker injection zones with greater vertical permeability provide more space for CO_2 to disperse vertically. This vertical dissipation of pressure helps limit the lateral extent of the pressure disturbance, thereby limiting the AoR size.

High-density brines typically result in a CO_2 plume-defined AoR (see Figure 4B). The pressure buildup required to cause leakage of dense brines up a wellbore or permeable pathway is higher compared to less dense fluids, due to the increased buoyancy force acting on the denser brine. The static mass-balance calculations (see Eq 1 and 2) show that the minimum reservoir pressure increase required to lift the denser brine continuously up a wellbore is higher compared to a less dense brine. The threshold pressure depends on factors like the density difference between the brine and wellbore fluid and the vertical distance over which the brine needs to be lifted from the bottom of the USDW to the top of the freshwater aquifer. For high brine densities, the pressure buildup required for leakage is high enough only in the proximity of the injection well, that the AoR, being the maximum of the plume and the critical pressure radius, ends up being plume-defined. Hence, highly saline aquifers are preferred, purely from the standpoint of minimizing the radius of the AoR. The exception is when the reservoir permeability is low, or the distance between the bottom of the USDW and the top of the reservoir is small. Reservoirs with low permeability and tiny and poorly connected pore throats impede the flow of CO_2 and lead to a pressure buildup extending over a larger area around the wellbore, leading to a critical pressure-defined AoR. Likewise, in formations with close vertical proximity between the USDW and the reservoir, the pressure buildup required for leakage is small (see Eq.1 and 2), and often occurs at a large distance from the injection well, beyond the plume, leading to a critical pressure-defined AoR.

As injection rates increase (see Figure 4c), the critical pressure radius increases more rapidly than the radius of the CO_2-saturated region and defines the AoR. Hence, for a given injection volume requirement, multiple injection wells each with lower injection rates may be more favorable than a single well with a high injection rate, to optimize the radius of the AoR. Increasing thickness and increasing permeability have a similar effect on the size of the AoR but to different extents (see Figure 6). The reservoir thickness has a comparatively milder influence on the AoR size than the permeability. A thicker reservoir may have a larger pore volume to accommodate the injected CO_2, but this does not greatly affect the extent of the pressure perturbation and the associated AoR. Reservoir permeability, on the other hand, has a much more pronounced effect in determining the AoR size. Higher permeability allows the injected CO_2 to propagate farther from the injection well while keeping the pressure buildup low, and the AoR small. In low permeability reservoirs, the CO_2 plume is more localized around the injection well, resulting in greater pressure buildup and a larger AoR.

The plot of AoR versus permeability follows a non-monotonic trend for low permeabilities (see Figure 4D) as a consequence of the Theis equation (Theis 1935). As permeability increases from very low values, the critical pressure radius grows rapidly initially, because higher permeability allows for easier fluid flow through the porous medium, enabling the pressure disturbance to propagate further into the formation. After reaching a peak, the critical pressure radius decreases with increasing permeability as pressure dissipates rapidly in highly permeable formations. The non-monotonicity in the relationship could help identify a "worst-case" permeability value that leads to the largest size of the AoR, all else being equal. The increasing separation between the bottom of the USDW and the top of the reservoir leads to a larger range of permeabilities for which the AoR is plume-governed (see Figure 7). Again, the hydrostatic mass-balance equations (see Eq 1 and 2) indicate that the minimum pressure buildup required to lift brine continuously up a wellbore is proportional to the vertical separation between the USDW and reservoir. For large separations, the pressure buildup required for leakage is high enough only in the proximity of the injection well, that the AoR, being the maximum of the plume and the critical pressure radius, ends up being plume-defined for higher permeabilities. It is only for extremely low permeabilities where the AoR is critical pressure-governed due to the large pressure buildup. A large vertical separation

between the USDW and reservoir thus not only minimizes the AoR but also minimizes the risk of contamination by providing sufficient permeability barriers that impede brine migration towards the USDW.

Developers often need to estimate the size of the AoR when the project is at its early stage, to determine the number of wells needing review and remediation, the acreage required, and the financial resources required for monitoring and corrective action. The phase diagram provides developers with a tool to predict whether the AoR is CO_2 plume or critical pressure-dominated based on the geological properties of the reservoir and injection rates. It also provides a way to compute the minimum change in kh/Q required for a project to move from the critical pressure-dominated region to the CO_2 plume-dominated region of the phase diagram. The nomogram, in addition to providing an estimate of the size of the AoR relative to the CO_2 plume, also enables developers to estimate the change in injection rate required to achieve a target radius of the AoR. These tools can be used for site selection and screening without building complex computational models to estimate AoR size.

Reservoir heterogeneity is expected to have a relatively minor influence at large distances from the injection well [see Fig. 10 and 11]. Near the injection well, heterogeneity can play a more significant role in influencing the preferential migration pathways of the injected CO_2 and the dissipation of pressure. However, these effects diminish with increasing distance and the overall response is more heavily dictated by the reservoir's average properties rather than localized heterogeneities.

Summary

Class VI well permit applications are often subjected to strict scrutiny leading to several stages of review that normally include a completeness review (~ 30 days), technical review (~ 18 months), draft permit preparation (~ 60 days), public comment period (~ 30 to 45 days), and the release of the final permit decision (~ 90 days), leading to an estimated total duration of up to 2 years ("UIC Class VI Wells Permit Tracker Dashboard" 2024).

Determining the AoR is a crucial early step in planning a CCS project, and needs to be continually evaluated as site characterization progresses and CO_2 injection plans are developed. The size of the AoR can impact the amount of acreage that needs to be acquired, as well as the cost of corrective actions if there are any nearby wells or faults.

CCSNet has greatly simplified the process of early-stage project characterization by providing results 10^3 to 10^4 times faster than conventional numerical simulators (Wen, Hay, and Benson 2021). The parametric tool developed using CCSNet as part of this study also provides developers with an interface to observe the variation of the plume, critical pressure, and the AoR radius as a function of permeability, injection rate, brine density, and reservoir thickness.

When considering injection rates and reservoir permeability and thickness for geological storage, a few factors come into play to optimize the AoR and minimize potential risks. Low injection rates and thicker, highly permeable reservoirs are preferred to keep the pressure buildup low and minimize the radius of the AoR. This approach allows for better control of the CO_2 plume and reduces the likelihood of unwanted migration or leakage.

From the standpoint of minimizing the radius of the AoR, highly saline aquifers are preferred for CO_2 storage. These aquifers typically have lower economic utility and are less likely to be used for other purposes, making them ideal candidates for long-term CO_2 sequestration.

When faced with a given injection volume requirement, utilizing multiple injection wells, each with lower injection rates may be more favorable, rather than a single well with a high injection rate. This strategy helps distribute the CO_2 more evenly throughout the reservoir, reducing localized pressure buildup and minimizing the risk of fracturing or compromising the integrity of the storage formation.

A large vertical separation between the USDW and the storage reservoir serves dual purposes. It not only minimizes the AoR but also significantly reduces the risk of contamination. This separation provides sufficient permeability barriers that impede

brine migration towards the USDW, ensuring the protection of valuable freshwater resources.

Near the injection well, where the CO_2 plume is concentrated, heterogeneity in the reservoir can play a more significant role in influencing the preferential migration pathways of the injected CO_2 and pressure buildup. Understanding and accounting for these heterogeneities is crucial for accurate modeling and prediction of CO_2 movement and pressure buildup within the storage formation, allowing for better risk assessment and management of the injection process.

The nomogram provides a set of curves that serve as a quick reference for the graphical computation of the radius of the AoR, while the phase diagram identifies the critical frontier with a transition between a plume-governed AoR and a pressure-governed AoR.

Clustering CO_2 sources and sinks through hubs is essential for CCS projects to achieve economies of scale. A key component to the success of hub projects is using a robust site selection framework to assess the suitability of a location for carbon sequestration (Callas et al. 2022). The authors believe that the size of the AoR is an important factor in determining the success of a project and should be integrated into the existing framework for CCS site selection.

It is also to be noted that CCSNet's reservoir-scale 2D isotropic model was used to run the trials. CCSNet has since undergone significant upgrades, with the addition of a reservoir-scale 2D anisotropic model and a basin-scale 3D model. These models present additional benefits including the ability to model multiple injection wells and greater flexibility in choosing parameters, which would allow for the development of more sophisticated parametric tools and charts for predicting AoR radii and governance in the future.

Code and data availability:

The Python notebooks used to connect to CCSNet's backend API, analyze the data, and build the parametric tool along with the data files and the CCS project tracker are available at https://github.com/hemanthhariharan/CCS_RA.

Links to specific Python notebooks:

- Connecting to CCSNet and running trials:
  https://github.com/hemanthhariharan/CCS_RA/blob/main/CCS_RA_AoR_trials.ipynb
- Parametric tool and data analysis:
  https://github.com/hemanthhariharan/CCS_RA/blob/main/CCS_RA_AoR_data_analysis.ipynb
- CCS project tracker:
  https://github.com/hemanthhariharan/CCS_RA/blob/main/CCS_project_tracker_GitHub.xlsx

References:

Benson, S.M., Cook, P., Anderson, J., Bachu, S., Nimir, H. B., Basu, B., Bradshaw, J., Deguchi, G., ... & Zhou, D. (2005). Underground geological storage. Cambridge University Press.

Gupta, S., & Li, L. (2022). The potential of machine learning for enhancing CO2 sequestration, storage, transportation, and utilization-based processes: a brief perspective. *Jom*, *74*(2), 414-428.

Hussin, F., Rahim, S. A. N. M., Hatta, N. S. M., Aroua, M. K., & Mazari, S. A. (2023). A systematic review of machine learning approaches in carbon capture applications. *Journal of CO2 Utilization*, *71*, 102474.

Li, N., Feng, W., Yu, J., Chen, F., Zhang, Q., Zhu, S., ... & Li, Y. (2023). Recent advances in geological storage: trapping mechanisms, storage sites, projects, and application of machine learning. *Energy & Fuels*, *37*(14), 10087-10111.

Pawar, R., Dempsey, D., & Guthrie, G. (2017). Effect of permeability heterogeneity on area of review. *Energy Procedia*, *114*, 7459-7465.

Remy, N., Boucher, A., & Wu, J. (2009). *Applied geostatistics with SGeMS: A user's guide*. Cambridge University Press.

Wang, Y., Chu, H., & Lyu, X. (2024). Deep learning in CO2 geological utilization and storage: Recent advances and perspectives. *Advances in Geo-Energy Research*, *13*(3), 161-165.

Bacon, Diana H., Deniz I. Demirkanli, and Signe K. White. 2020. "Probabilistic Risk-Based Area of Review (AoR) Determination for a Deep-Saline Carbon Storage Site." *International Journal of Greenhouse Gas Control* 102 (November):103153. https://doi.org/10.1016/j.ijggc.2020.103153.

Bielicki, Jeffrey M., Julie K. Langenfeld, Zhiyuan Tao, Richard S. Middleton, Anne H. Menefee, and Andres F. Clarens. 2018. "The Geospatial and Economic Viability of CO2 Storage in Hydrocarbon Depleted Fractured Shale Formations." *International Journal of Greenhouse Gas Control* 75 (August):8–23. https://doi.org/10.1016/j.ijggc.2018.05.015.

Birkholzer, Jens T., Jean Philippe Nicot, Curtis M. Oldenburg, Quanlin Zhou, Stephen Kraemer, and Karl Bandilla. 2011. "Brine Flow up a Well Caused by Pressure Perturbation from Geologic Carbon Sequestration: Static and Dynamic Evaluations." *International Journal of Greenhouse Gas Control* 5 (4): 850–61. https://doi.org/10.1016/j.ijggc.2011.01.003.

Bump, Alexander P., and Susan D. Hovorka. 2023. "Minimizing Exposure to Legacy Wells and Avoiding

Conflict between Storage Projects: Exploring Area of Review as a Screening Tool." *International Journal of Greenhouse Gas Control* 129 (October):103967. https://doi.org/10.1016/j.ijggc.2023.103967.

Callas, Catherine, Sarah D. Saltzer, J. Steve Davis, Sam S. Hashemi, Anthony R. Kovscek, Esuru R. Okoroafor, Gege Wen, Mark D. Zoback, and Sally M. Benson. 2022. "Criteria and Workflow for Selecting Depleted Hydrocarbon Reservoirs for Carbon Storage." *Applied Energy* 324 (October):119668. https://doi.org/10.1016/j.apenergy.2022.119668.

Celia, Michael A., Jan M. Nordbotten, Benjamin Court, Mark Dobossy, and Stefan Bachu. 2011. "Field-Scale Application of a Semi-Analytical Model for Estimation of CO2 and Brine Leakage along Old Wells." *International Journal of Greenhouse Gas Control* 5 (2): 257–69. https://doi.org/10.1016/j.ijggc.2010.10.005.

Intergovernmental Panel on Climate Change. 2015. *Climate Change 2014: Mitigation of Climate Change: Working Group III Contribution to the IPCC Fifth Assessment Report*. Cambridge: Cambridge University Press. https://doi.org/10.1017/CBO9781107415416.

Millero, Frank J., Chen-Tung Chen, Alvin Bradshaw, and Karl Schleicher. 1980. "A New High Pressure Equation of State for Seawater." *Deep Sea Research Part A. Oceanographic Research Papers* 27 (3): 255–64. https://doi.org/10.1016/0198-0149(80)90016-3.

Nicot, Jean-Philippe, Curtis M. Oldenburg, Steven L. Bryant, and Susan D. Hovorka. 2009. "Pressure Perturbations from Geologic Carbon Sequestration: Area-of-Review Boundaries and Borehole Leakage Driving Forces." *Energy Procedia*, Greenhouse Gas Control Technologies 9, 1 (1): 47–54. https://doi.org/10.1016/j.egypro.2009.01.009.

Theis, Charles. 1935. "The Relation between the Lowering of the Piezometric Surface and the Rate and Duration of Discharge of a Well Using Ground-Water Storage." *Eos, Transactions American Geophysical Union* 16 (2): 519–24.

Tsang, C. F., Benson, S. M., Kobelski, B., & Smith, R. E. (2002). Scientific considerations related to regulation development for CO 2 sequestration in brine formations. *Environmental Geology*, *42*, 275-281.

"UIC Class VI Wells Permit Tracker Dashboard." 2024. May 24, 2024. https://awsedap.epa.gov/public/single/?appid=8c074297-7f9e-4217-82f0-fb05f54f28e7&sheet=51312158-636f-48d5-8fe6-a21703ca33a9&theme=horizon&bookmark=6218ffed-bb6e-42e4-a4f1-52d87e036a1b&opt=ctxmenu.
US EPA. 2013. Geologic Sequestration of Carbon Dioxide Underground Injection Control (UIC) Program Class VI Well Area of Review Evaluation and Corrective Action Guidance. https://www.epa.gov/sites/default/files/2015-07/documents/epa816r13005.pdf

US EPA. 2015. "Class VI - Wells Used for Geologic Sequestration of Carbon Dioxide." Overviews and Factsheets. May 12, 2015. https://www.epa.gov/uic/class-vi-wells-used-geologic-sequestration-carbon-dioxide.

Wen, Gege, Catherine Hay, and Sally M. Benson. 2021. "CCSNet: A Deep Learning Modeling Suite for CO2 Storage." *Advances in Water Resources* 155 (September):104009. https://doi.org/10.1016/j.advwatres.2021.104009.

Acknowledgments: